

Pacific climate influences on ocean conditions and extreme shell growth events in the Northwestern Atlantic (Gulf of Maine)

Alan D. Wanamaker Jr. ¹ · Shelly M. Griffin · Caroline C. Ummenhofer · Nina M. Whitney · Bryan Black · Rhys Parfitt · Erin E. Lower-Spies · Douglas Introne · Karl J. Kreutz

Received: 24 March 2018 / Accepted: 19 October 2018 / Published online: 25 October 2018 © Springer-Verlag GmbH Germany, part of Springer Nature 2018

Abstract

The Gulf of Maine is undergoing rapid environmental and ecological changes, yet our spatial and temporal understanding of the climatic and hydrographic variability in this region, including extreme events, is limited and biased to recent decades. In this study, we utilize a highly replicated, multi-century master shell growth chronology derived from the annual increments formed in the shells of the long-lived bivalve *Arctica islandica* collected in 38 m from the central coastal region in the Gulf of Maine. Our results indicate that shell growth is highly synchronous and inversely related to local seawater temperatures. Using composite analyses of extreme shell growth events from CE 1900 to 2013, we extend our understanding of the factors driving oceanic variability and shell growth in the Northwestern Atlantic back to CE 1761. We suggest that extreme shell growth events are primarily controlled by Gulf of Maine sea surface temperature (SST) and stratification conditions, which in turn appear to be largely influenced by SST patterns in the Pacific Ocean through their influence on mid-latitude atmospheric circulation patterns and the location of the eddy-driven jet. The large-scale jet dynamics during these extreme years manifest as precipitation and moisture transport anomalies and regional SST conditions in the Gulf of Maine that either enhance or inhibit shell growth. Pacific climate variability is thus an important, yet understudied, influence on Gulf of Maine ocean conditions.

 $\textbf{Keywords} \ \ Gulf \ of \ Maine \cdot Extreme \ events \cdot Pacific \ Decadal \ Oscillation \cdot ENSO \cdot Teleconnection \cdot Eddy-driven \ jet \cdot Sclerochronology \cdot Crossdating \cdot Chronology \cdot Shell \ growth$

Electronic supplementary material The online version of this article (https://doi.org/10.1007/s00382-018-4513-8) contains supplementary material, which is available to authorized users.

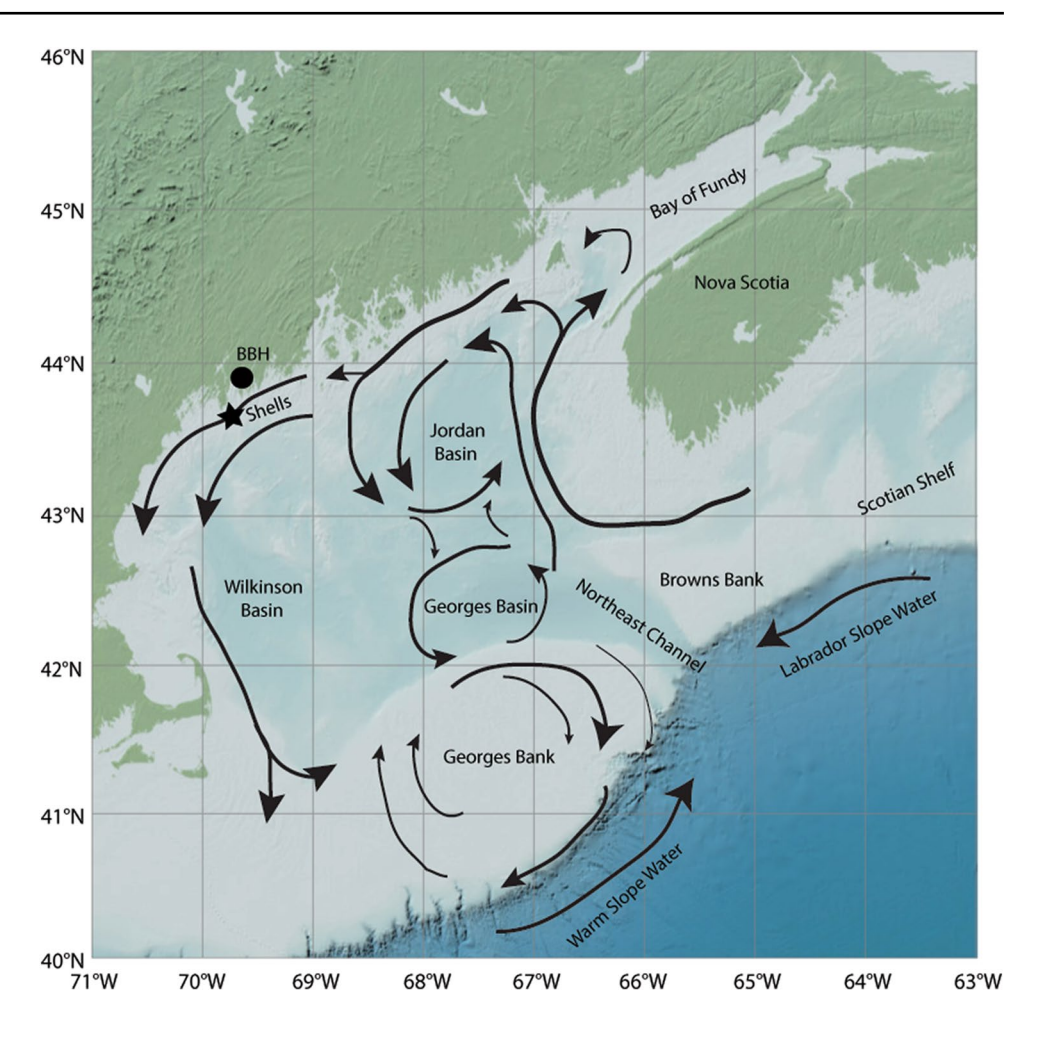
- Alan D. Wanamaker Jr. adw@iastate.edu
- Department of Geological and Atmospheric Sciences, Iowa State University, Ames, IA 50011, USA
- Department of Physical Oceanography, Woods Hole Oceanographic Institution, Woods Hole, MA 02543, USA
- Jaboratory of Tree-Ring Research, University of Arizona, Tucson, AZ 85721, USA
- School of Earth and Climate Sciences and Climate Change Institute, University of Maine, Orono, ME 04469, USA

1 Introduction

The Gulf of Maine (GoM) is a highly productive and economically important mid-latitude sea situated in the Northwestern Atlantic Ocean (Fig. 1) (for a review see Townsend et al. 2006) that is undergoing rapid environmental and ecological changes (Dijkstra et al. 2017). For example, based on satellite data, Pershing et al. (2015) concluded that the GoM surface waters warmed faster than 99% of the global ocean during the period from 1982 to 2013. Using this same data set (but including 2014), Thomas et al. (2017) noted increasing summer duration, as defined by regional sea surface temperature (SST) thresholds, over the last three decades in the GoM and surrounding region. As a global marine "hotspot" (Hobday and Pecl 2014) the northwest Atlantic is highly susceptible to enhanced warming in the future (Saba et al. 2016). In addition to warming, the GoM is particularly vulnerable to ocean acidification (Ekstrom et al. 2015), the combination of which poses serious threats



Fig. 1 The general Gulf of Maine surface circulation (adapted from Pettigrew et al. 2005) is shown. The location of our study site (Seguin Island) is noted with a star symbol. The location of the Boothbay Harbor (BBH) seawater instrumental records is noted with a solid circle symbol



to GoM fisheries, especially Atlantic cod stocks and shellfish (Pershing et al. 2015; Ekstrom et al. 2015).

Despite its importance for supporting diverse biota and ecosystems, the general biological, chemical, and physical oceanographic conditions prior to the twentieth century in the GoM are not well known. Furthermore, few studies to date have investigated the frequency of extreme events in the GoM region, such as the tilefish kill in 1892 and the extreme warming of 2012, and/or the potential dynamical causes of such events (Marsh et al. 1999; Chen et al. 2014). Hence our understanding of the drivers of extreme events and the impacts of these events on GoM ecosystems is incomplete. Although several studies have demonstrated remote forcing of GoM environmental conditions within the Atlantic basin (e.g., Petrie and Drinkwater 1993; Greene and Pershing 2003; Wanamaker et al. 2008a; Nye et al. 2011; Pershing et al. 2015), potential climate linkages and/or teleconnections outside the region, including the Pacific Ocean, have rarely been explored.

A more comprehensive understanding of the past oceanographic and climatic behavior may provide a rich context for understanding recent changes in GoM ecosystems (e.g., Pershing et al. 2015; Townsend et al. 2015; Krumhansl et al. 2016; Dijkstra et al. 2017). Even though Boothbay Harbor in the central GoM is home to one of the longest SST records in the USA (1905–present; see note by Drinkwater and Petrie 2011), our understanding of temporal and spatial variability in oceanographic conditions, especially subsurface, is limited. Thus proxy-based techniques (e.g., Jones et al. 2009), including the analysis of growth increments in the hard parts of long-lived marine organisms such as bivalves, corals, fishes, and sclerosponges (see Schöne and Surge 2005; Gröcke and Gillikin 2008; Oschmann 2009; Wanamaker et al. 2011a; Schöne and Gillikin 2013; Butler and Schöne 2017; Prendergast et al. 2017) are needed to extend our knowledge of past marine conditions.

To maximize proxy accuracy, an increasing number of studies have applied the dendrochronology technique of crossdating (Douglas 1941; Fritts 1971) to establish master growth chronologies from annual increments in long-lived marine biota (Butler et al. 2009a, b, 2013; Black et al. 2008, 2009; Griffin 2012; Mette et al. 2016). As in dendrochronology, the prevailing hypothesis in sclerochronology (growth-increment analysis in calcified hard parts) is that



some aspect of the environment (e.g., seawater temperature, food quality/availability, stratification) varies over time and influences growth, thereby inducing synchronous growth patterns analogous to a "bar code" among many individuals of a given species and location. Crossdating is the process of matching these patterns back through time beginning with the outermost increment formed at the known year of death and proceeding toward the center. So doing ensures that all increments, including micro- or false-increments, have been correctly identified. Thus, accurately crossdating multiple individuals from a location (see Black et al. 2016 for a review) ensures that the master growth chronology is free of temporal error and fully retains high frequency information including the frequency and magnitude of extreme events. Such master chronologies also can serve as a foundation to explore growth (Strom et al. 2004; Black et al. 2009) and geochemical variations through time and space (e.g., Mette et al. 2016; Reynolds et al. 2016) and their relationships to environmental conditions.

In this study, we develop a well-replicated, crossdated chronology from annual increment widths of the marine bivalve *Arctica islandica* collected from the GoM. The objectives of this work are to (1) quantify the degree of growth synchrony among individuals, (2) establish the regional environmental drivers of this synchronous growth, (3) reconstruct this variability, including its spectral properties, over the full extent of the chronology. Given the annual resolution of the chronology, an additional objective is to (4) quantify the background, long-term frequency of extreme events for comparison with the modern record. Of particular interest is the potential influence of Pacific climate variability on these extremes via large-scale teleconnection patterns in the atmosphere that change the regional circulation, moisture transport, and eddy-driven jet in the GoM region.

2 Background and methods

2.1 Study site

Source waters to the GoM (Fig. 1) include relatively shallow Scotian Shelf Water and Maine River Water, as well as relatively deep Labrador Slope Water and Warm Slope Water (Gatien 1976; Smith 1983; Chapman and Beardsley 1989; Brown and Irish 1993; Pettigrew et al. 2005; Khatiwala et al. 1999; Houghton and Fairbanks 2001). Warm Slope Water is warmer and more saline and nutrient rich compared to Labrador Slope Water (Townsend and Ellis 2010). Townsend et al. (2015) provide a detailed review of water masses and nutrient sources to the GoM in additional to schematic representations of surface and bottom currents in the region. Pettigrew et al. (2005) described the GoM Coastal Current, which is largely counterclockwise (Fig. 1) and heavily

influenced by Maine River Water. This current is characterized by two principal branches: the upstream Eastern Maine Coastal Current, which extends from Nova Scotia (Canada) to Penobscot Bay, and the Western Maine Coastal Current, which flows from Penobscot Bay to Cape Cod (Massachusetts) (Pettigrew et al. 2005; Manning et al. 2009). The study site, located in the seawater surrounding Seguin Island, is located approximately 4 km offshore from Popham Beach State Park (Maine, USA) and is situated in the Western Maine Coastal Current (Fig. 1). Seguin Island is also located near the mouth of the Kennebec River, one of the region's larger river systems with a catchment of ~9500 km² (Michor 2003). Based on nearby buoys (B01, Western Maine Shelf and E01, Central Maine Shelf; see http://www.neracoos.org/ gomoos), this part of the Western Maine Coastal Current is highly stratified in summer, less stratified in spring and fall, and fully vertically mixed in the winter.

2.2 Arctica islandica Proxy Archive

The long-lived bivalve mollusk Arctica islandica (Fig. S1), common in the shelf seas of the temperate to sub-polar North Atlantic Ocean, is an excellent high-resolution marine archive with considerable potential in oceanography and climate studies (for a review, see Schöne 2013). This stationary benthic clam lives in water depths ranging from ~5 m to as deep as 500 m and thrives in full marine conditions, yet can also tolerate salinities as low as 28 PSU for short time intervals (Nicol 1951; Merrill and Ropes 1969; Mette et al. 2016). A. islandica clams live within the sediment and extend their relatively short siphons into the main water column exchanging water to feed and remove waste. A. islandica is highly suitable for environmental and ocean studies because: (1) it is extremely long-lived - up to 500 years (Schöne et al. 2005; Wanamaker et al. 2008b; Butler et al. 2013); (2) it produces annual growth increments in its shell (Jones 1980; Scourse et al. 2012); (3) regional increment series can be crossdated, demonstrating a common response to environmental forcing(s) (Butler et al. 2009a, b, 2010, 2013); (4) dead-collected shells can be crossdated and floating shell chronologies can be constructed after radiocarbon dating (Scourse et al. 2006); (5) live-caught shells can be crossdated with dead-collected shells to assemble very long, absolutely dated growth records (Marchitto et al. 2000; Butler et al. 2010, 2013); and (6) master shell growth chronologies can be created that are as statistically robust as tree ring chronologies (Butler et al. 2010; Marali and Schöne 2015; Mette et al. 2016; Bonitz et al. 2018).



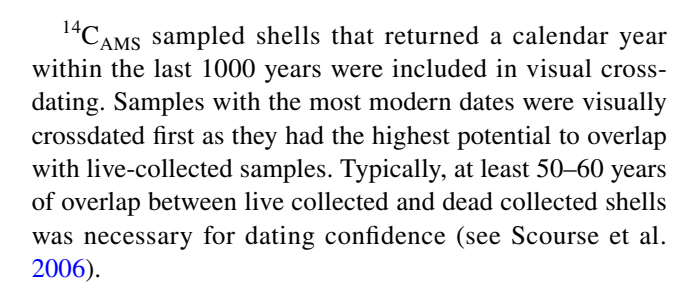
2.3 Sample collection, preparation, and radiocarbon dating

Live and dead specimens of *A. islandica* were collected near Seguin Island (43.714151°N, 69.751652°W; Fig. 1) at a depth of 38 m using a scallop dredge aboard F.V. Nothin' Serious III in 2010, 2011, 2012, and 2014. The sampling location was selected based on the availability of specimens and its proximity to long-term environmental monitoring stations, located at Boothbay Harbor, which is approximately 16 km to the northeast of Seguin Island. Soft tissues were removed from live-caught clams and shell samples were shipped to Iowa State University.

In order to facilitate chronology building (also see supplementary information for detailed description; Figs. S1 and S2), dead-collected shell samples (often large and always well preserved) were processed for radiocarbon analysis (14C) at the NOSAMS (National Ocean Sciences Accelerator Mass Spectrometry) facility at the Woods Hole Oceanographic Institution (Table S1). The surface of each shell was cleaned by scraping it with a razor blade, and the periostracum, if intact, was removed prior to sampling. Approximately 10 mg of aragonite powder was collected from each shell using a hand drill at the lowest speed. The shell was sampled from a known location such that the sample could be temporally referenced to the appropriate calendar years. Radiocarbon analysis was used to establish their "rough" date of death. Of the shells measured for ¹⁴C activity, ~50% apparently lived during the last millennium. This estimate only considers a normal marine radiocarbon reservoir effect of about 400 years (e.g., Wanamaker et al. 2012).

2.4 Visual crossdating

Visual crossdating was completed prior to any measurement of growth increments (see Stokes and Smiley 1996; Speer 2010) by viewing samples under the microscope as well as panoramic digital images. Whenever possible, increments from the hinge and margin were both visually crossdated (Fig. S2). The clearest (i.e., easiest to read) acetate peels from live-collected animals were initially selected for visual crossdating. These were often the smallest, youngest shells (<30 years) with the largest growth increments. Progressively larger (and older) shells were added, extending the chronology back in time. Crossdating proceeded from the outermost increment formed during the known year of capture toward the innermost increment formed during the first year of life using skeleton plotting and list-year techniques (Yamaguchi 1991; Stokes and Smiley 1996). Intrashell comparisons between the hinge and margin were helpful to identify mistakes such as missed micro- or false-rings (Fig. S2B, C, D) before performing intershell comparisons.



2.5 Measuring and chronology construction

Each annual increment was measured perpendicular to the increment boundaries using Buehler OmniMet software (v9.5) (Fig. S2B, C). Increment boundaries were easier to distinguish at relatively low magnifications (i.e., $2 \times$ and $5 \times$) in clams less than 100 years old. As increments became smaller and more compressed in older clams, higher magnifications were used $(10 \times, 20 \times)$.

After the shells were visually crossdated and measured, crossdating was statistically verified using the MatLab script SHELLCORR (Scourse et al. 2006). In this script, each measurement time series is fit with a 15-year, 50% frequency cutoff cubic spline and then divided by the values predicted by the function. This removes low-frequency variability, isolating high-frequency variability that meets the assumptions of correlation analysis (Holmes 1983). Moreover, the detrended time series were log transformed to reduce the influence of any extreme growth years on correlation values (see Butler et al. 2013). Next, these detrended and logtransformed time series were correlated against one another in pairwise comparisons. Correlations were performed in 21-year running windows to ensure that the entire time series was correctly aligned: a missed or falsely added increment would appear as a sudden drop in correlation beginning at the point in time at which the error occurred. SHELLCORR was also used to calculate correlations across a range of lag and leads (± years) as a way to determine the number of years with which two time series were misaligned should a dating (or measurement) error have occurred (Butler et al. 2009b).

The program COFECHA was used as an additional statistical check of crossdating accuracy (Holmes 1983; Grissino-Mayer 2001). Similar to SHELLCORR, high-frequency patterns are isolated within each measurement time series and these detrended, log-transformed time series are correlated among one another (Holmes 1983). However, each detrended measurement time series is correlated with the average of all others (as opposed to pairwise correlations; Grissino-Mayer 2001). The mean of these is reported as the interseries correlation.

Once crossdating had been visually and statistically verified, a final master shell growth chronology was constructed using the dendrochronology program ARSTAN (version



40c, available at http://www.ltrr.arizona.edu/software.hmtl; Cook 1985). All shell growth series were detrended with a negative exponential curve to remove ontogenetic growth trends. This detrending technique was selected because it removes the age related growth decline while still retaining as much low-frequency variability as possible (see Butler et al. 2010, 2013). The master shell growth chronology was constructed using a biweighted robust mean to minimize the effect of outliers (Cook et al. 1990). The strength of chronology was assessed by calculating the expressed population signal (EPS), which measures the extent to which the chronology represents the theoretical population from which samples were drawn (Wigley et al. 1984). Although arbitrary, an EPS > 0.85 is considered adequate for climate reconstruction. Note that multiple time series from the same individual were averaged prior to calculating the EPS (Wigley et al. 1984). EPS and mean pairwise correlations (rbar), were calculated using ARSTAN.

2.6 Seawater temperature and Kennebec River discharge data

Observational seawater temperature data were obtained from Boothbay Harbor (BBH; Maine, USA; Fig. 1), which is ~16 km away from Seguin Island (Fig. 1). Records of BBH SST and -8 m (below mean low tide) seawater temperatures were obtained from the Maine Department of Marine Resources http://www.maine.gov/dmr/rm/environmentalda ta.html, by request. The SST record spans 1905-present with a short gap from 1949 to 1950. From 1905 to 2013, only 17 months are missing making the record 98.7% complete. The -8 m data span January 1989-March 2012, at which time the instrument failed. The near 24-year record (279 months) is 91% complete with 25 months of data missing. Only complete data for any given year or season were used in comparison with our master shell growth chronology. Monthly discharge data for the Kennebec River in Bingham, Maine $(45.05^{\circ}N, -69.88^{\circ}E)$ is available via the United States Geological Survey (https://waterdata.usgs.gov/ usa/nwis/uv?01046500) and spans the 1965–1983 interval.

2.7 Composite analyses of climatic conditions during extreme growth events

A series of monthly, global gridded observational and reanalysis products were used to assess climatic conditions during years exhibiting extreme shell growth. The data sets included precipitation at 0.5° horizontal resolution from the Global Precipitation Climatology Centre (GPCC; version 6; 1901–2010; Schneider et al. 2013); sea level pressure (SLP), zonal and meridional winds, and specific humidity at 2.5° horizontal resolution from the twentieth Century reanalysis (20CR; 1871–2011; Compo et al. 2011); and SST at 1°

horizontal resolution from the UK Hadley Centre HadISST (1870–present; Rayner et al. 2003). The common analysis period among the data sets was 1901–2010. The climatic analyses focus on the February–August months, when shell growth is most sensitive to environmental conditions. We use composite analyses (e.g., Andreu-Hayles et al. 2017) for precipitation, moisture transport, geopotential height at 500 hPa, SLP, and SST to explore the anomalous regional and large-scale climatic conditions associated with extreme shell growth years. Moisture transport in the atmosphere was calculated as the product of specific humidity and zonal as well as meridional winds at each level and then vertically integrated below 500 hPa.

Variability in the extratropical westerly flow over the North Atlantic is dominated by the eddy-driven jet, which is associated with momentum transport and areas of convergence/divergence that affect local weather and climatic conditions (e.g., Merz et al. 2015). The eddy-driven jet moves on daily to monthly time scales and exhibits preferred latitudinal locations on a seasonal basis. Here, we focus on its latitudinal position during the spring months (March–May; MAM), expressed as a percentage of days that the jet spends in a particular position, as this relates to synoptic conditions across the broader Northwest Atlantic region during the spring season that likely precondition shell growth in the GoM. The daily latitude of the North Atlantic eddy-driven jet is calculated using the zonal wind at 850 hPa for MAM drawing from an adapted methodology of Woollings et al. (2010). The daily zonal wind at 850 hPa at each longitude is smoothed with a 10-day low-pass Butterworth filter. The latitude at which the filtered zonal wind exhibits its maximum amplitude is identified as the dominant jet latitude for that day. To test where composite anomalies during extreme shell growth years were significant, a two-tailed student t test was used at the 90% confidence level.

2.8 Growth extremes

Extreme events were identified as years exhibiting the lowest 10% and highest 10% of detrended growth index (DGI) values during the instrumental period (1901–2010) (Andreu-Hayles et al. 2017). To determine extreme events for the entire master shell growth chronology, years with DGI values ≤ 0.50 and ≥ 1.47 were considered extreme, based on these extreme DGI values obtained for the instrumental period. The frequency of years with extreme DGI values was calculated as the number of these events per decade in 20-year sliding windows. A Monte Carlo or boot-strapping method was employed to assess whether the number of extreme years were unusual. In so doing, we randomly selected with replacement ten DGI values, repeated this 10,000 times, and calculated an expected distribution of the number of extreme high and low values per decade. A



decade in the chronology was considered significant when the observed frequency of extremes fell above or below the 95% or 5% level of the bootstrapped data, respectively.

To further assess persistent patterns in shell growth, we also used three independent techniques of spectral analyses: wavelet analysis (Torence and Compo 1998), multi taper method (MTM; Thomson 1982; Mann and Lees 1996), and singular spectrum analysis (SSA; Vautard and Ghil 1989). Each technique offers distinct advantages over traditional Blackman-Tukey analysis, which is susceptible to aliasing and requires several window lengths to extract dominant frequencies, and Fourier transforms, which are ineffective on non-stationary time series. Wavelet analysis decomposes a time-series into time-frequency space, which allows one to visualize dominant modes of variability and how those modes vary through time (Torence and Compo 1998). Further, wavelet transforms can be used to evaluate time-series that are non-stationary and contain a variety of frequencies (Daubechies 1990). MTM is a refined Fourier-based analysis that offers better resolution and decreased spectral leakage (Thomson 1982). SSA enables a time-series decomposition into trend, oscillating, and noise components by analyzing its covariance matrix (Vautard and Ghil 1989).

2.9 Pacific climate data

The master shell growth chronology was compared to monthly mean values of the Pacific Decadal Oscillation index (PDO; Mantua et al. 1997) over the 1900-2013 common interval (http://research.jisao.washington.edu/pdo/ PDO.latest.txt). Positive values of the PDO index indicate warm regime in which temperature anomalies along the west coast of North America are above average. The chronology was also compared to the Multivariate El Nino Southern Oscillation (ENSO) Index (MEI; 1950-present; https://www.esrl.noaa.gov/psd/enso/mei/), calculated as the first principal component of sea-level pressure, zonal and meridional surface wind, sea surface temperature, surface air temperature, and total cloudiness fraction of the sky in the tropical Pacific (Wolter and Timlin 1998). Positive values indicate El Nino conditions while negative values indicate La Nina conditions.

3 Results

3.1 Master shell growth chronology

The master shell growth chronology is defined as that period in which EPS exceeds 0.85 and spans the years 1761 to 2013. Minimum sample depth is four individuals, though 34 were



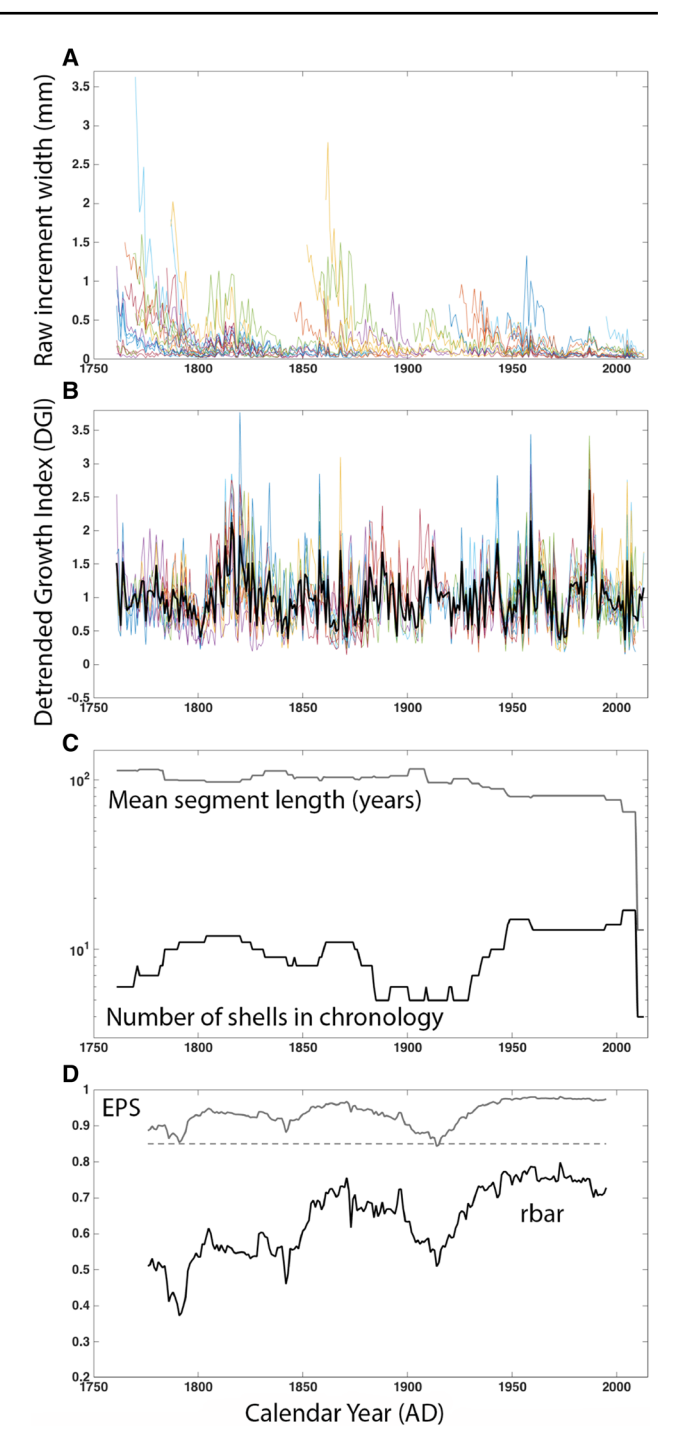


Fig. 2 a Raw increment width for all shell series. **b** Detrended shell growth series and the master shell growth chronology/detrended growth index (DGI) (heavy black line; units are standard deviations). **c** Mean segment length and number of shells in the chronology through time on a log scale. **d** Expressed population signal (EPS) and interseries correlations (rbar) using a 30-year window with a 29-year overlap. The recommended minimum EPS value (0.85) is shown as a dashed line

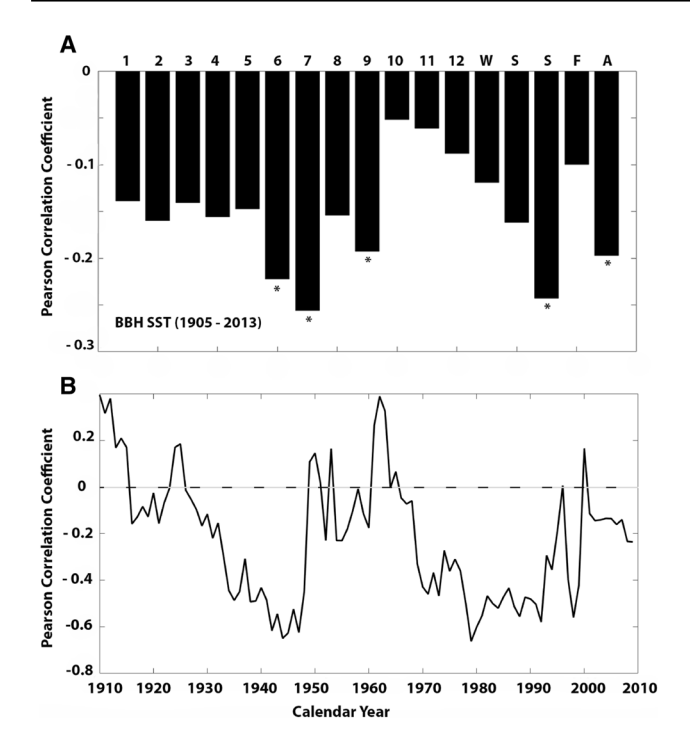


Fig. 3 a Relationships between the master shell growth chronology and BBH SST from 1905 to 2013. Statistically significant correlations at the 95% confidence level are noted by the asterisk symbol and account for the relative degrees of freedom (n-2) for each record. Months are shown as 1–12. Seasons are shown in order as W (winter; DJF), S (spring; MAM), S (summer; JJA), and F (fall; SON). Annual averages are noted as A. The strongest correlation between the master shell growth chronology and seawater temperature occurred for the summer average. **b** Temporal correlation using an 11-year moving average between the master shell growth chronology and summer Boothbay Harbor (BBH) SST is shown

used to generate the chronology (Fig. 2a, b), of which 21 were live-caught and 13 were dead-collected. Measurement from both the hinge and margin regions (intrashell replication) was completed on 53% of the shells. The mean segment length is 95.5 years with a range of 13–115 years. Average interseries correlation is 0.64 while mean sensitivity is 0.45.

3.2 Seawater temperature versus the master shell growth chronology

The chronology is weakly and inversely correlated to BBH SST (1905–2013) (Fig. 3). Only the months of June, July, and September are statistically significant (r = -0.19) to -0.26; p < 0.05). The annual average and summer (JJA) SSTs are also statistically significant despite being relatively weak (r = -0.20 to -0.24; p < 0.05). The strongest relationship during this interval is between shell growth and summer SSTs at BBH (r = -0.24; p < 0.05). However, the temporal correlation between shell growth and summer SST is fairly variable in strength and sign (Fig. 3) during the entire interval. When considering only the interval from 1989 to 2012, the length of the -8 m seawater temperature record at BBH, correlations are higher (Fig. 4), but levels of significance remain comparable to those identified for the full record given the reduced degrees of freedom. However, seasonality of climate response is somewhat different from the full record in that the winter and spring months of February, March, April, and May are significant, as is July (r = -0.41)to -0.51; p < 0.05). The spring season (r = -0.54; p < 0.05) was statistically significant and this seasonal relationship improves slightly by including February to the months of March, April, and May (r = -0.55; p < 0.05).

The relationship between BBH seawater temperatures at -8 m and the master shell growth chronology from 1989 to 2012 (omitting 1999 and 2004 due to missing data) is

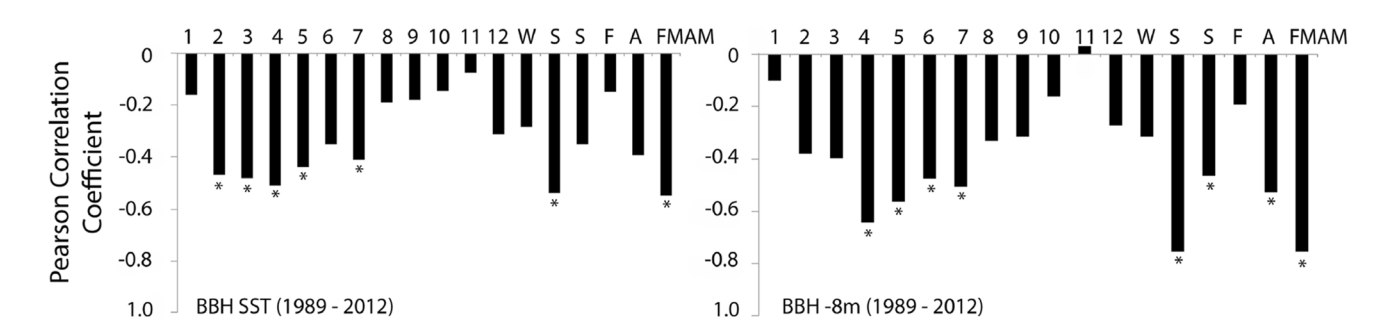


Fig. 4 Relationships between the master shell growth chronology and Boothbay Harbor (BBH) SST (left) and BBH -8 m seawater temperature (right) from 1989 to 2012. Statistically significant correlations at the 95% confidence level are noted by the asterisk symbol and account for the relative degrees of freedom (n-2) for each record. Months are shown as 1-12. Seasons are shown in order as W (winter;

DJF), S (spring; MAM), S (summer; JJA), and F (fall; SON). Annual averages are noted as A. The strongest correlations between the master shell growth chronology and seawater temperature occurred for the months of FMAM (2, 3, 4, 5) for both the surface and -8 m records



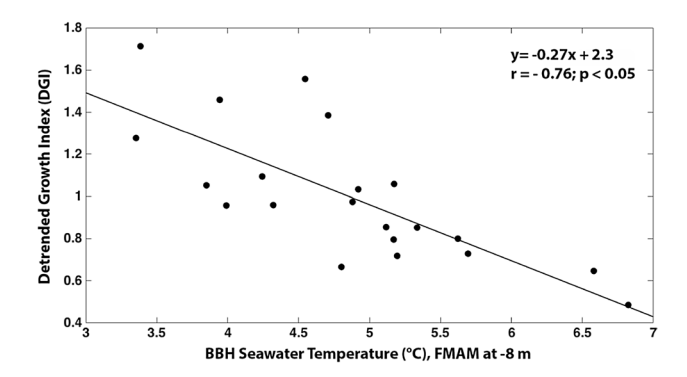


Fig. 5 The relationship between the detrended growth index (DGI) and Boothbay Harbor (BBH) -8 m seawater temperature record for the months of FMAM from 1989 to 2012 is shown

also negative, but substantially stronger than relationships with SST data, even over the same common interval (Fig. 4). The months of April, May, June, and July are statistically significant (r=-0.48 to -0.64; p<0.05). Spring (MAM; r=-0.75; p<0.05), summer (JJA; r=-0.47; p<0.05) and annual average (r=-0.53; p<0.05). The strongest correlation (r=-0.76; p<0.05) between shell growth and seawater temperatures at -8 m is with the mean of February through March (FMAM), which explains 58% of the chronology variance (Fig. 5).

3.3 Relationships between Kennebec River discharge, SST, and the master shell growth chronology

Annual Kennebec River discharge from 1965 to 1983 (19 years) was significantly related to SSTs at BBH (r=0.62; p<0.005) and also with the master shell growth chronology (r=-0.49; p=0.04, with a maximum correlation from April to March, r=-0.55; p=0.02).

3.4 Extreme shell growth composite analysis (CE 1900–2013) and associated climatic conditions

The ten highest and lowest shell growth years are indicated in the time series of the detrended growth index shown in Fig. 6a (also see Table S2). During the period that overlaps with the instrumental record (CE 1900–2013), high growth extremes are evenly distributed, while low growth extremes are absent prior to 1930 and between 1980 and 2000 (Fig. 6). A cluster of low growth extremes occurred from the late 1960s through the mid 1970s (Fig. 6).

Climatic conditions from February to August, the likely period over which *A. islandica* grow in the GoM (see Beirne et al. 2012), were used for the composite analyses. Extreme high shell growth years were characterized by negative precipitation anomalies (Fig. 6b) with northerly and offshore

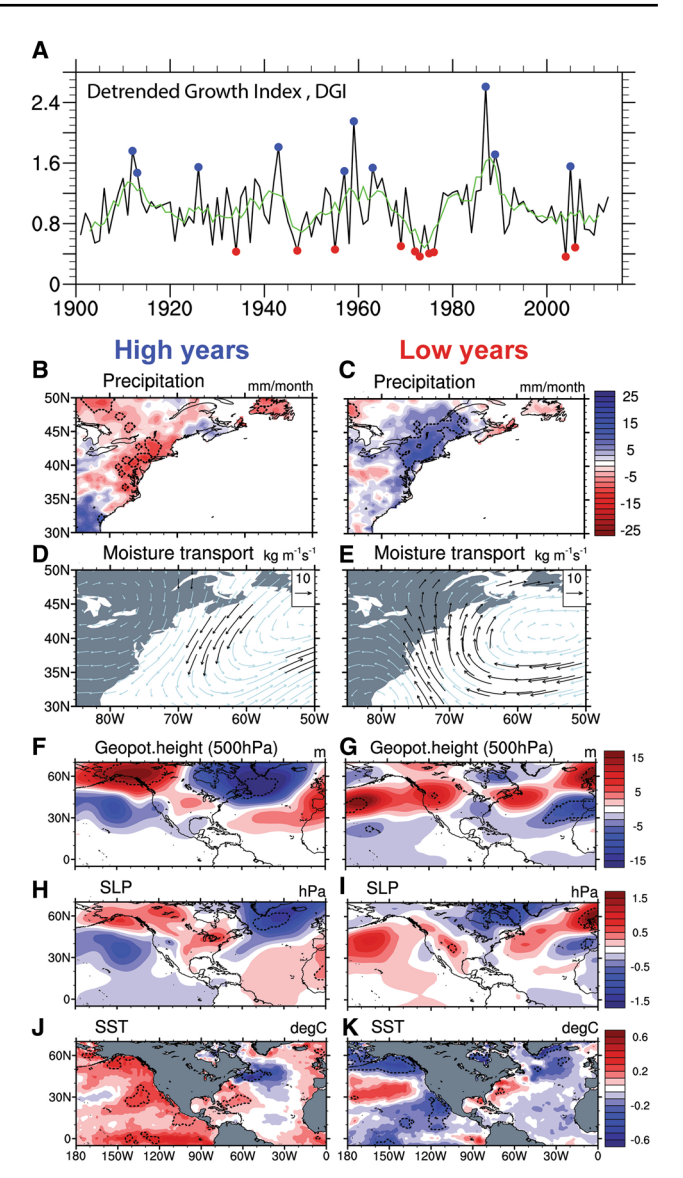


Fig. 6 a Composite analyses of the detrended growth index (DGI) from CE 1900 to 2013, whereby the ten most extreme high (low) shell growth events are shown in blue (red). The green line is a 5-year smoothing filter. **b, c** Precipitation anomalies (mm/month) during extreme high and low shell growth events. **d, e** Moisture transport anomalies (kg/m/s) during extreme high and low shell growth events. **f, g** Geopotential height anomalies (m) at 500 hPa during extreme high and low shell growth events. **h, i** Sea level pressure (SLP) anomalies (hPa) during extreme high and low shell growth events. **j, k** Sea surface temperature (SST) anomalies (°C) during extreme high and low shell growth events. Significant anomalies at the 90% confidence level are delimited by black dashed lines (black arrows in **d, e**)

moisture transport anomalies (Fig. 6d). At broader spatial scales, hemispheric anomalies in 500 hPa geopotential height (Fig. 6f) are apparent in a characteristic Rossby wave train pattern emanating from the Pacific to higher latitudes across the North American continent. Positive SLP anomalies occurred over the Gulf of Alaska, across northern



Canada into New England, while negative SLP anomalies were centered in the Northeast Pacific (25°N–45°N, 150°W) and the region south of Greenland and Iceland, extending into the North Atlantic region as far south as Bermuda (Fig. 6h). These years were also characterized by anomalously warm SST (>+0.5 °C) in the Northeastern Pacific, especially along the coast of western North America. In the Atlantic, cool SST anomalies extended from the GoM region offshore via the Gulf Stream extension, past the Grand Banks region towards south of Greenland (Fig. 6j). In contrast, extreme low shell growth years are broadly characterized by the opposite climatic conditions from those during high growth years, including 500 hPa geopotential height anomalies, SLP and SST of the North Pacific (Fig. 6c, e, g, i, k). Indeed, the general state of the North Pacific, especially with respect to the contrast between central and coastal regions of the basin, is consistent with opposite phases of the PDO (Mantua et al. 1997; Newman et al. 2016) during the two sets of years. For low shell growth years, warm SST anomalies were seen along the eastern US coastline from Florida to Nova Scotia (Fig. 6k), while anomalously cool SST appeared in the central subpolar North Atlantic extending from south of Greenland to the Grand Banks offshore of Newfoundland. Chen and Kwon (2018) investigated the mechanism behind an observed negative correlation between Pacific decadal variability associated with the PDO and oceanic conditions on the Atlantic Northwest shelf, including the GoM: they found it to be primarily due to variability in radiative fluxes,

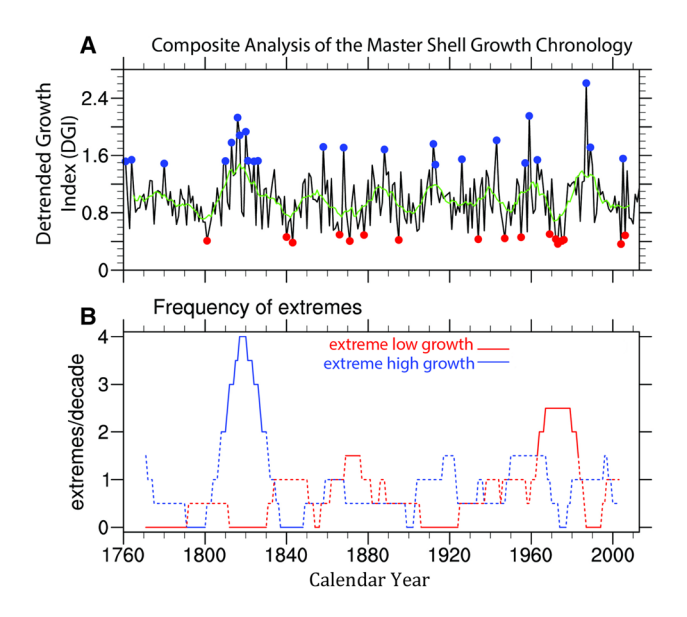


Fig. 7 a Composite analyses of the detrended growth index (DGI) from CE 1761 to 2013; extreme high (low) shell growth events are shown in blue (red). The green line is a 10-year smoothing filter. **b** Frequency of extreme shell growth events (extremes per decade); extreme high (low) shell growth events are shown in blue (red)

mostly related to short- and long-wave radiation in response to changed cloud cover over the Northwest Atlantic.

3.5 Extreme events since CE 1761

The growth thresholds to define extreme growth years from CE 1900–2013 were applied to the entire record (Fig. 7; Table S2). A total of 24 extreme high shell growth years occurred, while only 16 extreme low shell years occurred in the 253-year chronology. By design, the rate of extreme events from 1900 to 2013 (10 highest and 10 lowest events) was 0.9 extremes per decade. In comparison, prior to the twentieth century, the rate of extreme high and low shell growth events were on average 1.0 and 0.43 events per decade, respectively. The frequency of extreme high shell growth events peaked from 1810 to 1830 and remained below ~ 1.5 extremes per decade to present. Extreme low shell growth events generally were absent or infrequent until about 1840. Thereafter, these events occurred somewhat more regularly but at a low rate (< 1.5 extremes per decade). The most frequent occurrence of extreme low shell growth events happened in the late 1960s to the mid 1970s, with the most prominent cluster from CE 1972 to 1976.

Wavelet analysis revealed persistent, ~ 30 year periodicity that is statistically significant above the 95% confidence level throughout most of the record (Fig. 8). MTM and SSA analyses also yielded multidecadal [29.3 years (MTM) and 30.3 years (SSA)] and subdecadal (3.4 and 2.0 years) periods that are significant above the 95% confidence level (Fig. 8). Also illustrated by the wavelet analysis is a signal in the 2–4 years band consistent with MTM and SSA analyses. Periods greater than 32 years were not considered meaningful (see gray rectangles in Fig. 8) due to the segment length curse (for specific details, see Cook et al. 1995). This issue is discussed in more detail below.

3.6 Unusual climatic conditions during 1972–1976 CE

The years 1972–1976 CE stand out as a period with unprecedented clustering of low shell growth years in the record since 1761 CE. Here, we assess climatic anomalies during this unusual period, focusing on the spring (MAM) season, given the sensitivity of shell growth to these months (Fig. 4) and the coherence in the climate signal to these months, especially in the strong seasonal dependence of the atmospheric teleconnection between the PDO and GoM SST to the spring season (Chen and Kwon 2018). Climatological analyses for MAM of these years (1972–1976) reveal exceptionally strong anomalies in 500 hPa geopotential height and SLP, and SSTs in the Pacific and Atlantic, in addition to moisture transport and precipitation in the GoM region (Fig. 9). Conditions in the Pacific reveal a strong PDO

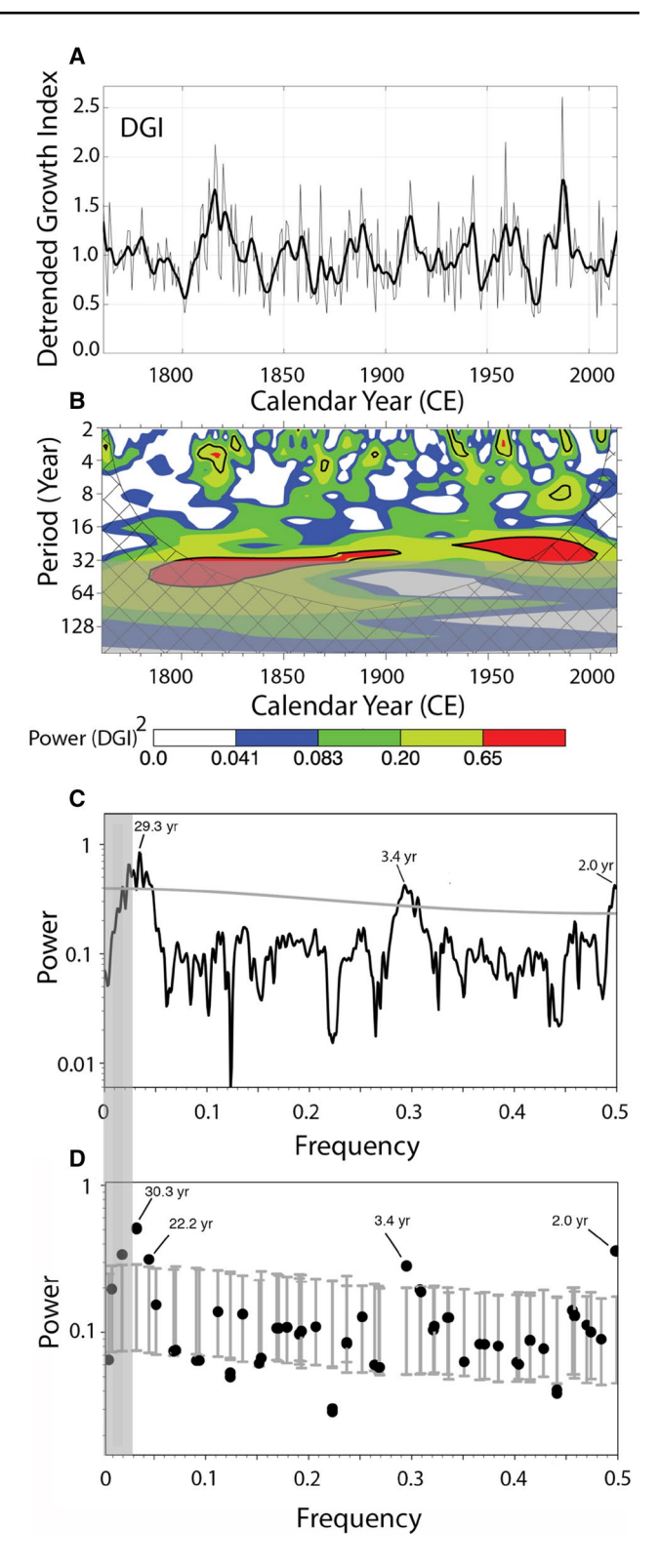


Fig. 8 a Master shell growth chronology/detrended growth index ▶ (DGI) (light black line) and a filtered version (smoothing spline: MatLab Curvefitting Toolbox, smoothing parameter: p=0.425) of the index are shown to highlight multidecadal variability. b Wavelet power spectrum of the detrended growth index (Morlet, parameter 6, start scale = 2, scale width = 0.25, powers-of-two = 11). The cross-hatched region is the cone of influence, where zero padding has reduced the variance. Black contour is the 95% confidence level, using a red-noise (autoregressive lag1) background spectrum (see Torence and Compo 1998). Periods greater than 32 years, illustrated by the gray rectangle, are not resolvable because of the segment length curse (see text). c Multi taper method (MTM) analysis of the detrended growth index [kSpectra version 3.4.3 using a red noise background (autoregressive lag1); resolution = 2; number of tapers = 3] is shown. Persistent periods are annotated on the plot that exceed the 95% confidence level, which is noted by the solid gray line. d Singular Spectrum Analysis (SSA) of the detrended growth index (kSpectra version 3.4.3; window = 60; covariance = V&G; significance = Chi-squared; components = 10) is shown. Persistent periods are annotated on the plot that exceed the 95% confidence level, are solid, black circles above the gray bars. For MTM and SSA analyses, the gray rectangle (left) is used to illustrate periods greater that 32 years, which are not considered resolvable

negative phase consistent with instrumental measures of the PDO (e.g., Mantua et al. 1997) and the associated extratropical remote teleconnections. Additionally, this interval was also indicative of fairly strong La Nina conditions (negative multivariate ENSO index). In the Atlantic, relatively warm SSTs and increased precipitation dominated conditions in the GoM.

Given the unusual conditions in the atmospheric circulation across the extratropical Northwest Atlantic during this low-growth period, it is of interest to investigate the characteristics of the eddy-driven jet across the North American/Atlantic sector, a hemispheric circulation feature that exhibits a dominant influence on cool-season weather and climate of the eastern seaboard of the US and the Northwest Atlantic. The latitudinal position of the eddy-driven jet varies from day to day and Fig. 10a shows the long-term average frequency of its position, expressed as a fraction of days for the spring (MAM) season for CE 1851-2014. Considering the preferred path of the jet, it is located most often near 40°N at 80°W and then has a slightly broader range in the 32°N-40°N range as it transitions from land to ocean (at ~75°W). From here, its preferred location gradually increases in latitude toward Europe, with a fairly large range in latitudinal distributions, although the highest frequencies of jet latitude are somewhat zonal in nature. A key feature of the jet is its preferred location (about 20% of the time) for the jet to be situated directly south of the GoM at about 40°N (Fig. 10a).

The frequency difference between the long-term eddy-driven jet (CE 1851–2014) for spring and the most extreme low shell growth cluster of the record (CE 1972–1976) is shown in Fig. 10b. This analysis reveals a more frequent northerly jet location in the GoM region and across the



Atlantic basin during this interval. A more northerly jet position during this cluster of low shell growth years is consistent with more frequent wetter and more unsettled weather conditions during spring, accounting for the higher



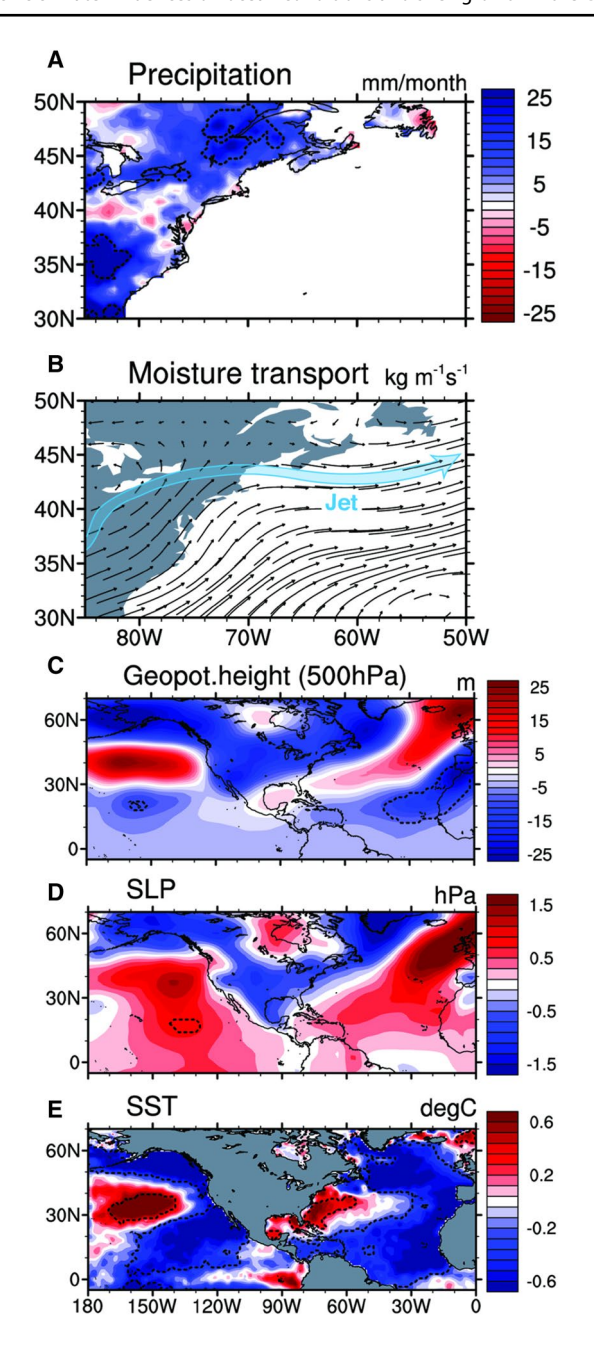


Fig. 9 Composite analyses for spring (MAM) of the detrended growth index (DGI) during the low growth cluster from CE 1972 to 1976. **a** Precipitation anomalies (mm/month) are shown. **b** Moisture transport anomalies (kg/m/s) are shown. **c** Geopotential height anomalies (m) at 500 hPa are shown. **d** Sea level pressure (SLP) anomalies (hPa) are shown. **e** Sea surface temperature (SST) anomalies (°C) are shown. Significant anomalies at the 90% confidence level are delimited by black dashed lines. The blue arrow in **b** is a schematic representation of the approximate preferred position of the eddy-driven jet during MAM for the period 1972–1976 CE. For the actual eddy-driven jet latitude frequency distribution see Fig. 10

precipitation anomalies (Fig. 9a) and runoff into the GoM that shells likely responded to (see Sect. 4.3).

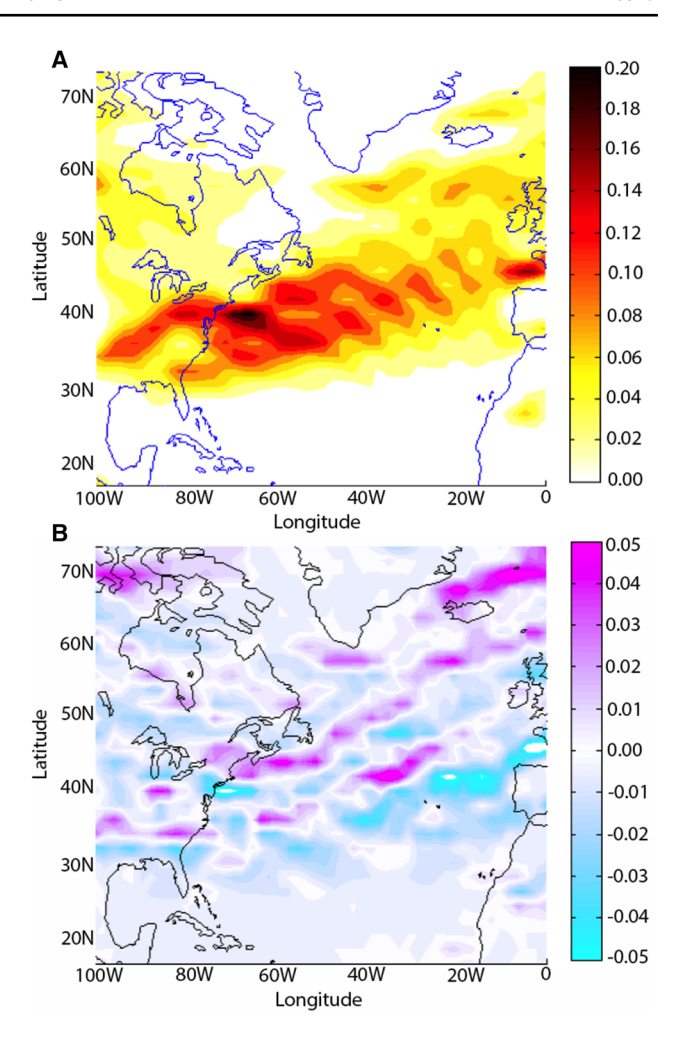


Fig. 10 a The frequency of the North Atlantic eddy-driven jet at 850 hPa, as a fraction of the total spring (MAM) period for 1851–2014. **b** The frequency difference (with frequency being calculated as a fraction of each respective period) between spring (MAM) 1972–1976 and spring 1851–2014. The difference is calculated as spring 1972–1976 minus spring 1851–2014, such that positive (negative) values indicate that the eddy-driven jet spends more (less) time in a given location for spring 1972–1976

3.7 Shell growth and Pacific climate (PDO and ENSO)

The PDO index was significantly (p < 0.05) and positively correlated to the master shell growth chronology (DGI values) in the months of April through July. The mean value for these months was significantly correlated to the chronology at r=0.28 (p=0.002). The MEI was positively and significantly correlated (p < 0.05) with the chronology from March through May. The mean value for these months was significantly correlated with the chronology at r=0.27 (p=0.03). These results indicate a weak but persistent influence of Pacific climate (consistent with PDO and ENSO variability) on oceanographic condition in the GoM, which in turn appears



to impact yearly shell growth in the GoM. Local conditions in the GoM are dependent in part on conditions in the Pacific because of changes to atmospheric flow and thus air-sea heat exchange in the GoM. However, the relationship between GoM oceanic conditions and Pacific climate could also be non-linear or non-stationary through time illustrating the benefit of using composite analyses on the master shell growth chronology.

4 Discussion

4.1 Master shell growth chronology

Interseries correlations and mean sensitivity are comparable to those described in other Arctica islandica chronologies, which are based in the northeastern Atlantic (Butler et al. 2013; Mette et al. 2016). Indeed, these values are high relative to that of other bivalve species or sclerochronological or dendrochronological series (Black 2009; Black et al. 2009, 2016). This high degree of synchrony suggests strong external forcing by environmental variability and facilitated crossdating and thus the accuracy of the final chronology. Without crossdating, the error of a single misidentified increment can "frame shift" the entire measurement time series by one year back through time, which can substantially attenuate the signal in the final chronology. This is particularly detrimental to retaining high-frequency variability and extreme events (Black et al. 2016). We found that intrashell comparisons (between the hinge and growing margin) greatly improved our ability to crossdate in this sample set given that it greatly reduced errors prior to intershell comparisons.

4.2 Long-term growth dynamics

A common problem in dendroclimatology is the loss of low-frequency environmental variability in tree-ring increment time series while removing ontogenetic growth trend. Known as the "segment length curse," periods that are longer than $\sim 1/3$ of the mean segment length are lost when detrending with negative exponential (or regression) functions (Cook et al. 1995). These same challenges are also characteristic of bivalve sclerochronology. Alternative detrending techniques are available (i.e., regional curve standardization (RCS); Esper et al. 2002; Butler et al. 2010) to preserve a greater portion low frequency variability in such time series, but this technique requires a large sample set of dead-collected samples that evenly span the study period. In this study, we did not have a sufficiently large dead collection and were further limited by using measurements from both the hinge and margin region to increase our sample size. However, with larger sample sizes, RCS approaches will be possible, as has been demonstrated in other *Arctica* sample sets (Butler et al. 2010), as will almost certainly be the case in the GoM with additional collections.

Given our mean segment length (95.5 years), only periods less than ~32 years would be theoretically valid. The three spectral analyses (wavelet, MTM, SSA) performed here revealed a robust periodicity of ~30 years in the master shell growth chronology in addition to relatively shorter periods (2 and 3.4 years). The spectral analyses suggest that these multidecadal and interannual periodicities are consistent along the length of the record, which suggests that they may have some predictive power as to future shell growth and ecosystem processes. Importantly, much of the spectral variability in shell growth is similar to that in Pacific climate variability (such as the PDO; 20-30 years; Mantua et al. 1997; Biondi et al. 2001 and ENSO; 3.5 and ~5 years; Deser 2012). Direct correlations with the patterns centered in the Atlantic region, including the North Atlantic Oscillation (interannual spectral power; Wallace and Gutzler 1981; Hurrell 1995; Gámiz-Fortis et al. 2002) and the Atlantic Multidecadal Oscillation (60-80 years; Delworth and Mann 2000; Sutton and Hodson 2005) indices with the master shell growth chronology did not reveal any statistically significant relationships. Hence, the 3.4 year peak in the master shell growth chronology (Fig. 8) is more indicative of ENSO variability rather than variability associated with the North Atlantic Oscillation. Given that the period associated with the Atlantic Multidecadal Oscillation is longer than 32 years, we are unable to determine if this signal is prevalent in shell growth.

4.3 Processes driving A. islandica shell growth in the Gulf of Maine

It is generally thought that food quantity and quality controls the growth of marine bivalves (Witbaard 1997; Witbaard et al. 1997; Saraiva et al. 2012), though relatively few studies have demonstrated a robust link between the two, largely due to a lack of observing networks at depth. However, in northern Norway, Ballesta-Artero et al. (2017) deployed a lander device with A. islandica clams in about 15 m water depth to monitor shell gaping activity. The lander was equipped to measure seawater temperature, salinity, chlorophyll-a concentrations, turbidity, and light conditions. Ballesta-Artero et al. (2017) reported that gaping activity among A. islandica clams was highly synchronous throughout the year, and that extended periods of gaping activity occurred when food was apparently available (i.e., elevated concentrations of chlorophyll-a). Further, gaping activity reached a maximum turbidity levels were also low. In this scenario, not only was ample



food available, but the clams did not expend excess resources filtering suspended sediment that was not energetically beneficial (Ballesta-Artero et al. 2017). These results suggest that growth, in concert with gaping activity, will be tightly linked to food quality. It is also important to note that Mette et al. (2016) found that *A. islandica* shell growth in northern Norway was inversely related to seawater temperature, which is in turn inversely related to productivity.

In this study, shell growth is inversely correlated with both local seawater temperatures and Kennebec River discharge. There may be two mechanisms for the sign of this relationship, the first being water-column stratification and its effect on food quality or quantity. Indeed, elevated SSTs and relatively high river input would both act to increase stratification at the study site. Stratification, in turn, would likely isolate food in the surface layer from the water below the thermocline and thereby reduce food export to the benthos. Effects of temperature and discharge are likely amplified given that SSTs and BBH are positively correlated. Thus, when SSTs are elevated, Kennebec River discharge is also likely high such that both contribute to stratification. In further support of the importance of food supply, high levels of primary productivity generally occur in the spring months in the GoM when seawater temperatures are relatively cool (e.g., Song et al. 2011). This time of year coincides with the seasons for which climate-growth relationships are strongest in this GoM chronology.

A second possible mechanism underlying an inverse temperature-growth relationship is that summertime temperatures approach the maximum thermal tolerance of this species, which is about 16 °C (Mann 1982). Indeed, Mann (1982) reported an ideal thermal range for A. islandica is from 6° to 10 °C, which has been supported by laboratory studies (e.g., Hiebenthal et al. 2012). Growth at higher temperatures is often at reduced rates. For example, growth of juvenile A. islandica clams (n=3) in a controlled experiment in the GoM was seven times higher at 10 °C (0.0091 mm/ day) versus 15 °C (0.0013 mm/day) (Milano et al. 2017). Similarly, Wanamaker and Gillikin (2018) reported growth rates in juvenile A. islandica clams (n = 5) that were 1.60 times higher at 10 °C compared to 15 °C. In the GoM, mean monthly seawater temperatures at the BBH -8 m station exceed 10 °C in June, July, August, September, and October, which could reduce growth rates in these summer and fall months.

Ultimately, both water-column stratification and thermal maxima likely have a combined influence on A. islandica growth given that peak levels of stratification likely co-occur with thermal maxima. These thermal controls are relatively strong given that seawater temperature at -8 m from February to May accounts for 58% of the master chronology over their common interval of 1989-2012 (a total of 21 years when accounting for missing data). Although the depth of

the -8 m station at BBH is not ideal considering that our shells were collected in -38 m, the relationships between shell growth and seawater temperatures at -8 m are substantially stronger than the surface. If SST reflects the degree of stratification, then ambient temperature appears to be much more relevant to explaining growth. Although an inverse relationship between shell growth and local seawater temperatures may not seem intuitive, Mette et al. (2016) also found a similarly negative relationship in northern Norway for which SST explained 12–52% of yearly *A. islandica* shell growth. Ongoing work with *A. islandica* growth in northern Norway using dynamic energy budget modeling (Ballesta-Artero, personal communication) will likely elicit a better understanding of the factors contributing to shell growth in Maine and Norway.

4.4 Frequency and causes of extreme shell growth events in the Gulf of Maine

As noted earlier, the frequency of extreme low shell growth years, which are associated with warm SST years (Figs. 6, 7) were most abundant in the twentieth century. The occurrence of extreme high shell growth years peaked from 1820 to 1830 during the late Little Ice Age (Wanamaker et al. 2011b), and these events are associated with cool SST (Figs. 6, 7). An increase (decrease) in extreme low (high) shell growth events is consistent with recent warming of the surface waters in the GoM noted by Pershing et al. (2015) and consistent with SST trends at BBH (see Drinkwater and Petrie 2011).

Ultimately, marine conditions that control salinity, seawater temperature, stratification dynamics, food availability/ quality within the GoM influence shell growth. We hypothesize that extreme shell growth events are primarily controlled by GoM stratification and SST conditions, which in turn impact vertical mixing and nutrient fluxes to the benthos. Coincident with cool SST conditions in the GoM, there is also decreased freshwater input from the Kennebec River catchment and overall drier conditions at the study site. These conditions are conducive to decreased seasonal stratification/increased vertical mixing, increased export of food to the benthos, less thermal stress/metabolic demand on the clams, and thus greater shell growth. Conversely, there is increased freshwater input from the Kennebec River catchment when warm SST conditions occur in the GoM, and overall wetter conditions at the study site (Fig. 6). These conditions would lead to increased seasonal stratification/ decreased vertical mixing, decreased export of food to the benthos, more thermal stress/metabolic demand on the clams, and thus less shell growth.

The spectral properties of shell growth led to investigating the possibility of Pacific influence on marine conditions in the GoM region. While the average correlation



between our master shell growth chronology and the PDO index (1900–2013) is low (r = 0.28; p = 0.002), it does reveal a persistent influence of Pacific climate on GoM shell growth. Similarly, the year to year correlation with ENSO (MEI; 1950-2013) and the master shell growth chronology is weak low (r = 0.27; p = 0.03). However, ENSO-like variability appears to be a persistent feature in the spectral domain (Fig. 8). Nevertheless, the climate-growth correlations for the full chronology with the PDO and ENSO are much weaker compared to those of the extreme years (composite analysis). Thus, the composite analyses made climate-growth relationships more obvious (extreme years tend to have the most leverage on shell growth) and further provided the means to identify and refine the teleconnection from the Pacific to the Atlantic. Indeed, the climatic conditions during extreme shell growth events appear to be largely influenced by SST conditions in the Pacific Ocean through their influence on mid-latitude geopotential height and SLP teleconnection patterns. Chen and Kwon (2018) found that the observed negative correlation between the PDO and SSTs over the Northwest Atlantic shelf had a strong seasonal dependence and was mainly driven by atmospheric variability impacting radiative fluxes in spring and ocean processes in summertime. Of particular relevance is that Chen and Kwon (2018) found that SSTs in the GoM region lagged those in the Pacific by 0–3 months during the spring and this lag increased slightly in the summer months, although some non-stationary behavior was noted. Previously, the authors had linked an exceptional warming event of the Northwest Atlantic shelf, including the GoM region, in 2011–2012 to atmospheric processes that affected radiative fluxes and were driven by unusual excursions in the atmospheric jet stream (Chen et al. 2014, 2015). Our analyses here have shown that the large-scale dynamics of the eddy-driven jet during extreme shell growth years lead to precipitation and moisture transport anomalies and regional SST conditions in the GoM that either enhance or inhibit shell growth in spring (Fig. 9). In particular, shell growth is inhibited during La Nina conditions and the negative phase of the PDO, which lead to warmer SSTs, positive precipitation anomalies, and increased stratification in the GoM. The most extreme case of low shell growth occurred from 1972 to 1976 during a prominent PDO negative phase/La Nina conditions (Fig. 9). Conversely, shell growth is enhanced when SSTs along the North American Pacific coastline are relatively warm (El Nino like). This proposed teleconnection leads to cooler SSTs, negative precipitation anomalies, and decreased stratification in the GoM. This teleconnection associated with Pacific climate yields climatic conditions in the GoM region that are consistent with our hypothesis regarding the role of SSTs, stratification dynamics, thermal maxima, and the export of food from the surface to the benthos.

Several studies have noted potential Pacific climate teleconnections to weather and climatic in the Northeastern United States and New England (e.g., Hubeny et al. 2011; Bradbury et al. 2002; Ning and Bradley 2015; Schulte et al. 2018; Schulte and Lee 2018). Some of these studies also infer a role in jet stream dynamics (position, waviness, persistence) to mechanistically link climatic conditions in the Northeastern United States to regions in the Northwestern United States and/or the Pacific. The eddy-driven jet location analyses conducted here (Fig. 10) support a role for the jet dynamics for modifying climatic conditions in the GoM, which ultimately are linked to these extreme shell growth events. Although Pershing et al. (2015) used the PDO index as an explanatory variable for SST conditions (from 1982 to 2013) in the GoM, they did not provide a physical explanation/mechanism for this use. Schulte et al. (2018) noted that seawater temperatures from Long Island Sound, south of the GoM, appear to be controlled by upstream atmospheric processes (i.e., jet stream dynamics). Specifically, Long Island Sound seawater temperatures appear to be negatively correlated with the PDO and eastern Pacific/North Pacific patterns, most notably during winter months (Schulte et al. 2018). Most recently, Chen and Kwon (2018) found that negative (positive) correlations in short- (long-)wave radiation, associated with variations in cloud cover over the Northwest Atlantic shelf, are the major contributors to the observed correlation with the PDO during spring. Based on the study of Pershing et al. (2015) the PDO was inversely correlated with SSTs in the GoM, explaining up to 25% of SST variations in the spring and ~45% of SST conditions in the summer from 1982 to 2013. Although we examined extreme shell growth events, our results are oceanographically consistent with those of Pershing et al. (2015). As illustrated in Fig. 6K, during a cool (negative) phase of the PDO, SSTs are higher in the GoM region. This result and those reported by others (Pershing et al. 2015; Schulte et al. 2018; Schulte and Lee 2018), strongly indicate a Pacific teleconnection to oceanographic conditions in the Northwestern Atlantic and especially in the GoM. For example, Schulte and Lee (2018) concluded that ENSO events influenced the onset and decay of extreme cooling of seawater temperatures within Long Island Sound. Interannual variability in shell growth in the GoM also has spectral properties consistent with ENSO dynamics, although the direct influence is fairly weak.

In summary, during strong PDO negative years/La Nina conditions, the GoM region may experience increased warming, which may have many cascading effects on fisheries and other ecosystems. Given the results noted here on extreme shell growth through time and the increased threats to fisheries and ecosystems in the GoM region due to ongoing (Pershing et al. 2015) and projected (Saba et al. 2016) warming, consideration of Pacific climate variability may give ecosystem managers in the Northwestern Atlantic an



additional tool to better prepare for future oceanographic conditions.

5 Conclusions

We have constructed a 253-year (CE 1761-2013) robust, absolutely-dated master shell growth chronology from annual increments of A. islandica shells collected in the GoM. Currently, this is the longest continuous sclerochronological record in the GoM and from the Northwestern Atlantic Ocean. The chronology includes a mixture of live-caught and dead-collected shells and we have demonstrated a strong link between shell growth and local seawater temperatures. Using composite analyses of extreme shell growth events during the twentieth century as a form of calibration, we extend our understanding of the factors driving shell growth and marine climate variability back to CE 1761 in the Northwestern Atlantic. We hypothesize that extreme shell growth events are primarily controlled by GoM stratification (impacting vertical mixing and nutrient fluxes) and SST conditions. Hydrographic conditions in the GoM seem to be largely influenced by SST conditions in the Pacific Ocean through their control on mid-latitude atmospheric circulation and SLP patterns, including the jet location. Specifically, we propose that the hemispheric dynamics of the eddy-driven jet during these extreme years lead to precipitation and moisture transport anomalies and regional SST conditions in the GoM that either enhance or inhibit shell growth. In particular, shell growth is inhibited during the negative phase of the PDO due to warmer SSTs, positive precipitation anomalies, and increased stratification in the GoM. Conversely, shell growth is enhanced when SSTs along the North American Pacific coastline are relatively warm leading to cooler SSTs, negative precipitation anomalies, and decreased stratification in the GoM. Extreme high shell growth (cool SST conditions in the GoM) reached a maximum from 1800 to 1840, while extreme low shell growth (warm SST conditions in the GoM) peaked in the late 1960s to the mid 1970s. The influence of Pacific climate variability, including ENSO, on ocean conditions in the GoM is an understudied, yet important, aspect contributing to anomalous oceanic conditions and extreme shell growth events.

Acknowledgements This work is funded by the National Science Foundation (OCE 1003438 and OCE 1003423) to ADW and KJK. CCU acknowledges financial support through NSF AGS-1602009 and the Investment in Science Fund given primarily by WHOI Trustee and Corporation Members. RP is funded by the Weston Howland Jr. postdoctoral scholarship at WHOI. We thank John Pinkham for (F.V. Nothin' Serious III) for his expertise in collecting shells, Robert Russell (Maine Department of Marine Resources) for sampling permits and assistance, and Heidi Bray (Maine Department of Marine Resources) for temperature data from Boothbay Harbor. Use of the following

data sets is gratefully acknowledged: Global Precipitation Climatology Center data set by the German Weather Service (DWD) through http://gpcc.dwd.de; Hadley Centre HadISST by the UK Met Office; and the Twentieth Century Reanalysis Project supported by the U.S. DOE, Office of Science Innovative and Novel Computational Impact on Theory and Experiment program, Office of Biological and Environmental Research, and NOAA Climate Program Office. We thank two anonymous reviewers for their detailed comments and constructive criticism that greatly improved this manuscript.

References

- Andreu-Hayles L et al (2017) 400 years of summer hydroclimate from stable isotopes in Iberian trees. Clim Dyn 49:143–161. https://doi.org/10.1007/s00382-016-3332-z
- Ballesta-Artero I, Witbaard R, Carroll ML, van der Meer J (2017) Environmental factors regulating gaping activity of the bivalve *Arctica islandica* in Northern Norway. Mar Biol 164:116. https://doi.org/10.1007/s00227-017-3144-7
- Beirne EC, Wanamaker AD, Feindel SC (2012) Experimental validation of environmental controls on the δ13C of *Arctica islandica* (ocean quahog) shell carbonate. Geochim Cosmochim Acta 84:395–409. https://doi.org/10.1016/j.gca.2012.01.021
- Biondi F, Gershunov A, Cayan DR (2001). North Pacific decadal climate variability since 1661. J Clim 14:5–10. https://doi.org/10.1175/1520-0442(2001)014%3C0005:NPDCV S%3E2.0.CO:2.
- Black BA (2009) Climate-driven synchrony across tree, bivalve, and rockfish growth-increment chronologies of the northeast Pacific.

 Mar Ecol Prog Ser 378:37–46. https://doi.org/10.3354/meps07854
- Black BA, Gillespie DC, MacLellan SE, Hand CM (2008) Establishing highly accurate production-age data using the tree-ring technique of crossdating: a case study for Pacific geoduck (*Panopea abrupta*). Can J Fish Aquat Sci 65:2572–2578. https://doi.org/10.1139/f08-158
- Black BA, Copenheaver CA, Frank D, Stuckey MJ, Kormanyos RE (2009) Multi-proxy reconstructions of northeastern Pacific sea surface temperature data from trees and Pacific geoduck. Palaeogeogr Palaeoclimatol Palaeoecol 278:40–47
- Black BA et al (2016) The value of crossdating to retain high-frequency variability, climate signals, and extreme events in environmental proxies. Glob Change Biol 22:2582–2595. https://doi.org/10.1111/gcb.13256
- Bonitz FGW, Andersson C, Trofimova T, Hátún H (2018) Links between phytoplankton dynamics and shell growth of *Arctica islandica* on the Faroe Shelf. J Mar Syst 179:72–87
- Bradbury JA, Dingman SL, Keim BD (2002) New England drought and relations with large scale atmospheric circulation patterns. J Am Water Resour Assoc 38:1287–1299. https://doi.org/10.1111/j.1752-1688.2002.tb04348.x
- Brown WS, Irish JD (1993) The annual variation of water mass structure in the Gulf of Maine: 1986–1987. J Mar Res 51:53–107. https://doi.org/10.1357/0022240933223828
- Butler PG, Schöne BR (2017) New research in the methods and applications of sclerochronology. Palaeogeogr Palaeoclimatol Palaeoecol 465:295–299
- Butler PG, Wanamaker AD Jr, Scourse JD, Richardson CA, Reynolds DJ (2013) Variability of marine climate on the North Icelandic Shelf in a 1357-year proxy archive based on growth increments in the bivalve Arctica islandica. Palaeogeogr Palaeoclimatol Palaeoecol 373:141–151. https://doi.org/10.1016/j.palaeo.2012.01.016



- Butler PG et al (2009a) Accurate increment identification and the spatial extent of the common signal in five *Arctica islandica* chronologies from the Fladen Ground, northern North Sea. Paleoceanography. https://doi.org/10.1029/2008pa001715
- Butler PG, Scourse JD, Richardson CA, Wanamaker AD Jr (2009b)
 Continuous marine radiocarbon reservoir calibration and the
 13C Suess effect in the Irish Sea: results from the first multicentennial shell-based marine master chronology. Earth Planet
 Sci Lett 279:230–241. https://doi.org/10.1016/j.epsl.2008.12.043
- Butler PG, Richardson CA, Scourse JD, Wanamaker AD, Shammon TM, Bennell JD (2010) Marine climate in the Irish Sea: analysis of a 489-year marine master chronology derived from growth increments in the shell of the clam *Arctica islandica*. Quat Sci Rev 29:1614–1632. https://doi.org/10.1016/j.quascirev.2009.07.010
- Chapman DC, Beardsley RC (1989) On the origin of shelf water in the Middle Atlantic Bight. J Phys Oceanogr 19:384–391. https://doi.org/10.1175/1520-0485(1989)019%3C0384:OTOOS W%3E2.0.CO:2.
- Chen K, Kwon Y-O (2018) Does Pacific Variability Influence the Northwest Atlantic shelf temperature? J Geophys Res Oceans 123:4110–4131
- Chen K, Gawarkiewicz GG, Lentz SJ, Bane JM (2014) Diagnosing the warming of the Northeastern US Coastal Ocean in 2012: a linkage between the atmospheric jet stream variability and ocean response. J Geophys Res Oceans 119:218–227. https://doi.org/10.1002/2013jc009393
- Chen K, Gawarkiewicz G, Kwon Y-O, Zhang WG (2015) The role of atmospheric forcing versus ocean advection during the extreme warming of the Northeast US continental shelf in 2012. J Geophys Res Oceans 120:4324–4339. https://doi.org/10.1002/2014J C010547
- Compo GP et al (2011) The twentieth century reanalysis project. Q J R Meteorol Soc 137:1–28. https://doi.org/10.1002/qj.776
- Cook ER (1985) A time series analysis approach to tree ring standardization. Dissertation, University of Arizona
- Cook ER, Briffa KR, Shiyatov S, Mazepa V (1990) Estimation of the mean chronology. In: Cook KL (ed) Methods of dendrochronology. Applications in the environmental sciences. Kluwer Academic Publishers, Dordrecht, pp 123–132
- Cook ER, Briffa KR, Meko DM, Graybill DA, Funkhouser G (1995) The 'segment-length curse' in long tree-ring chronology development for palaeoclimatic studies. Holocene 5:229–237. https://doi. org/10.1177/095968369500500211
- Daubechies I (1990) The wavelet transform, time-frequency localization and signal analysis. IEEE Trans Inf Theory 36:961–1005. https://doi.org/10.1109/18.57199
- Delworth TL, Mann ME (2000) Observed and simulated multidecadal variability in the Northern Hemisphere. Clim Dyn 16:661–676. https://doi.org/10.1007/s003820000075
- Deser C et al (2012) ENSO and Pacific decadal variability in the community climate system model version 4. J Clim 25:2622–2651
- Dijkstra JA, Harris LG, Mello K, Litterer A, Wells C, Ware C, Hughes AR (2017) Invasive seaweeds transform habitat structure and increase biodiversity of associated species. J Ecol 105:1668–1678. https://doi.org/10.1111/1365-2745.12775
- Douglas AE (1941) Crossdating in dendrochronology. J Forest 39(10):825-831
- Drinkwater KF, Petrie B (2011) A note on the long-term sea surface temperature records at Boothbay Harbor, Maine. J Northwest Atl Fish Sci 43:93–101. https://doi.org/10.2960/J.v43.m663
- Ekstrom JA et al (2015) Vulnerability and adaptation of US shellfisheries to ocean acidification. Nat Clim Change 5:207–214. https://doi.org/10.1038/nclimate2508
- Esper J, Cook ER, Schweingruber FH (2002) Low-frequency signals in long tree-ring chronologies for reconstructing past temperature

- variability. Science 295:2250–2253. https://doi.org/10.1126/science.1066208
- Fritts HC (1971) Dendroclimatology and dendroecology. Quat Res 1:419–449
- Gámiz-Fortis SR, Pozo-Vázquez D, Esteban-Parra MJ, Castro-Díez Y (2002) Spectral characteristics and predictability of the NAO assessed through singular spectral analysis. J Geophys Res Atmos 107:ACL 11–ACL-15. https://doi.org/10.1029/2001jd001436
- Gatien M (1976) A study in the slope water region south of Halifax.

 J Fish Res Board Can 33:2213–2217. https://doi.org/10.1139/f76-270
- Greene CH, Pershing AJ (2003) The flip-side of the North Atlantic Oscillation and modal shifts in slope-water circulation patterns. Limnol Oceanogr 48(1):319–322
- Griffin SM (2012) Applying dendrochronology visual crossdating techniques to the marine bivalve *Arctica islandica* and assessing the utility of master growth chronologies as proxies for temperature and secondary productivity in the Gulf of Maine. Thesis, Iowa State University
- Grissino-Mayer HD (2001) Evaluating crossdating accuracy: a manual and tutorial for the computer program COFECHA. Tree Ring Res 57:205–221
- Gröcke DR, Gillikin DP (2008) Advances in mollusc sclerochronology and sclerochemistry: tools for understanding climate and environment. Geo Mar Lett 28:265–268. https://doi.org/10.1007/s00367-008-0108-4
- Hiebenthal C, Philipp EER, Eisenhauer A, Wahl M (2012) Interactive effects of temperature and salinity on shell formation and general condition in Baltic Sea *Mytilus edulis* and *Arctica islandica*. Aquat Biol 14:289–298. https://doi.org/10.3354/ab00405
- Hobday AJ, Pecl GT (2014) Identification of global marine hotspots: sentinels for change and vanguards for adaptation action. Rev Fish Biol Fish 24:415–425. https://doi.org/10.1007/s1116 0-013-9326-6
- Holmes RL (1983) Computer-assisted quality control in tree-ring dating and measurement. Tree Ring Bull 43:69–78
- Houghton RW, Fairbanks RG (2001) Water sources for Georges Bank. Deep Sea Res Part II 48:95–114. https://doi.org/10.1016/S0967 -0645(00)00082-5
- Hubeny JB, King JW, Reddin M (2011) Northeast US precipitation variability and North American climate teleconnections interpreted from late Holocene varved sediments. Proc Natl Acad Sci USA 108:17895–17900. https://doi.org/10.1073/pnas.1019301108
- Hurrell JW (1995) Decadal trends in the North Atlantic Oscillation: regional temperatures and precipitation. Science 269:676–679
- Jones DS (1980) Annual cycle of shell growth increment formation in two continental shelf bivalves and its paleoecological significance. Paleobiology 6:331–340. https://doi.org/10.1017/S0094 837300006837
- Jones PD et al (2009) High-resolution palaeoclimatology of the last millennium—a review of current status and future prospects. Holocene 19:3–49. https://doi.org/10.1177/0959683608098952
- Khatiwala SP, Fairbanks RG, Houghton RW (1999) Freshwater sources to the coastal ocean off northeastern North America: evidence from (H₂O)-O-18/(H₂O)-O-16. J Geophys Res Oceans 104:18241–18255. https://doi.org/10.1029/1999jc900155
- Krumhansl KA et al (2016) Global patterns of kelp forest change over the past half-century. Proc Natl Acad Sci 113:13785–13790. https://doi.org/10.1073/pnas.1606102113
- Mann R (1982) The seasonal cycle of gonadal development in *Arctica islandica* from the southern New England shelf. Fish Bull 80:315–326

- Mann ME, Lees JM (1996) Robust estimation of background noise and signal detection in climatic time series. Clim Change 33:409–445. https://doi.org/10.1007/BF00142586
- Manning JP, McGillicuddy DJ, Pettigrew NR, Churchill JH, Incze LS (2009) Drifter observations of the Gulf of Maine coastal current. Cont Shelf Res 29:835–845. https://doi.org/10.1016/j.csr.2008.12.008
- Mantua NJ, Hare SR, Zhang Y, Wallace JM, Francis RC (1997). A Pacific interdecadal climate oscillation with impacts on salmon production. Bull Am Meterol Soc 78:1069–1079. https://doi.org/10.1175/1520-0477(1997)078%3C1069:APICO W%3E2.0.CO;2.
- Marali S, Schöne BR (2015) Oceanographic control on shell growth of *Arctica islandica* (Bivalvia) in surface waters of Northeast Iceland—implications for paleoclimate reconstructions. Palaeogeogr Palaeoclimatol Palaeoecol 420:138–149
- Marchitto TM, Jones GA, Goodfriend GA, Weidman CR (2000)
 Precise temporal correlation of Holocene mollusk shells
 using sclerochronology. Quat Res 53:236–246. https://doi.
 org/10.1006/gres.1999.2107
- Marsh R et al (1999) The 1882 tilefish kill—a cold event in shelf waters off the north-eastern United States?. Fish Oceanogr 8:39–49. https://doi.org/10.1046/j.1365-2419.1999.00092.x
- Merrill AS, Ropes JW (1969) The general distribution of the surf clam and ocean quahog. Proc Natl Shell Fish Assoc 59:40–45
- Merz N, Raible CC, Woollings T (2015) North Atlantic eddy-driven jet in interglacial and glacial winter climates. J Clim 28:3977– 3997. https://doi.org/10.1175/JCLI-D-14-00525.1
- Mette MJ, Wanamaker AD, Carroll ML, Ambrose WG, Retelle MJ (2016) Linking large-scale climate variability with *Arctica islandica* shell growth and geochemistry in northern Norway. Limnol Oceanogr 61(2):748–764. https://doi.org/10.1002/lno.10252
- Michor DJ (2003) People in nature: environmental history of the Kennebec River, Maine. Thesis, University of Maine
- Milano S, Nehrke G, Wanamaker AD Jr, Ballesta-Artero I, Brey T, Schöne BR (2017) The effects of environment on *Arctica islandica* shell formation and architecture. Biogeosciences 14:1577–1591. https://doi.org/10.5194/bg-14-1577-2017
- Newman M et al (2016) The Pacific Decadal Oscillation, revisited. J Clim 29(12):4399–4427
- Nicol D (1951) Recent species of the veneroid pelecypod Arctica. J Wash Acad Sci 41:102–106
- Ning L, Bradley RS (2015) Influence of eastern Pacific and central Pacific El Niño events on winter climate extremes over the eastern and central United States. Int J Climatol 35:4756–4770. https://doi.org/10.1002/joc.4321
- Nye JA, Joyce TM, Kwon YO, Link JS (2011) Silver hake tracks changes in Northwest Atlantic circulation. Nat Commun 2:412. https://doi.org/10.1038/ncomms1420
- Oschmann W (2009) Sclerochronology: editorial. Int J Earth Sci 98:1–2. https://doi.org/10.1007/s00531-008-0403-3
- Pershing AJ et al (2015) Slow adaptation in the face of rapid warming leads to collapse of the Gulf of Maine cod fishery. Science 350:809–812. https://doi.org/10.1126/science.aac9819
- Petrie B, Drinkwater K (1993) Temperature and salinity variability on the Scotian Shelf and in the Gulf of Maine 1945–1990. J Geophys Res Oceans 98:20079–20089. https://doi.org/10.1029/93JC02191
- Pettigrew NR et al (2005) The kinematic and hydrographic structure of the Gulf of Maine coastal current. Deep Sea Res Part II 52:2369–2391. https://doi.org/10.1016/j.dsr2.2005.06.033
- Prendergast AL, Versteegh EAA, Schone BR (2017) New research on the development of high-resolution palaeoenvironmental proxies from geochemical properties of biogenic carbonates. Palaeogeog Palaeoclimatol Palaeoecol 484:1–6

- Rayner NA et al (2003) Global analysis of sea surface temperature, sea ice, and night marine air temperature since the late nine-teenth century. J Geophys Res. https://doi.org/10.1029/2002J D002670
- Reynolds DJ et al (2016) Annually resolved North Atlantic marine climate over the last millennium. Nat Commun 7:13502. https://doi.org/10.1038/ncomms13502
- Saba VS et al (2016) Enhanced warming of the Northwest Atlantic Ocean under climate change. J Geophys Res Oceans. https://doi. org/10.1002/2015JC011346
- Saraiva S, van der MM, Kooijman S, Witbaard R, Philippart CJM, Hippler D, Parker R (2012) Validation of a dynamic energy budget (DEB) model for the blue mussel *Mytilus edulis*. Mar Ecol Prog Ser 463:141–158. https://doi.org/10.3354/meps09801
- Schneider U, Becker A, Finger P, Meyer-Christoffer A, Ziese M, Rudolf B (2013) GPCC's new land surface precipitation climatology based on quality-controlled in situ data and its role in quantifying the global water cycle. Theor Appl Climatol 115:15–40. https://doi.org/10.1007/s00704-013-0860-x
- Schöne BR (2013) *Arctica islandica* (Bivalvia): a unique paleoenvironmental archive of the northern North Atlantic Ocean. Glob Planet Change 111:199–225. https://doi.org/10.1016/j.gloplacha.2013.09.013
- Schöne BR, Gillikin DP (2013) Unraveling environmental histories from skeletal diaries—advances in sclerochronology. Palaeogeogr Palaeoclimatol Palaeoecol 373:1–5. https://doi.org/10.1016/j. palaeo.2012.11.026
- Schöne BR, Surge D (2005) Looking back over skeletal diaries—highresolution environmental reconstructions from accretionary hard parts of aquatic organisms. Palaeogeogr Palaeoclimatol Palaeoecol 228:1–3. https://doi.org/10.1016/j.palaeo.2005.03.043
- Schöne BR, Fiebig J, Gleb R, Hickson J, Johnson ALA, Dreyer W, Oschmann W (2005) Climate records from a bivalved Methuselah (*Arctica islandica*, Mollusca; Iceland). Palaeogeogr Palaeoclimatol Palaeoecol 228:130–148. https://doi.org/10.1016/j. palaeo.2005.03.049
- Schulte JA, Lee S (2018) Long Island sound temperature variability and its associations with the ridge-trough dipole and tropical modes of sea surface temperature variability. Ocean Sci Discuss. https://doi.org/10.5194/os-2018-25
- Schulte JA, Georgas N, Saba V, Howell P (2018) North Pacific influences on long island sound temperature variability. J Clim 31:2745–2769
- Scourse JD et al (2006) First cross-matched floating chronology from the marine fossil record: data from growth lines of the long-lived bivalve mollusc *Arctica islandica*. Holocene 16:967–974. https://doi.org/10.1177/0959683606hl987rp
- Scourse JD et al (2012) The marine radiocarbon bomb pulse across the temperate North Atlantic: a compilation of Delta C-14 time histories from *Arctica islandica* growth increments. Radiocarbon 54:165–186. https://doi.org/10.1111/j.1502-3885.2010.00141.x
- Smith PC (1983). The mean and seasonal circulation off southwest Nova Scotia. J Phys Oceanogr 13:1034–1054. https://doi.org/10.1175/1520-0485(1983)013%3C1034:tmasco%3E2.0.co;2.
- Song H, Ji R, Stock C, Kearney K, Wang Z (2011) Interannual variability in phytoplankton blooms and plankton productivity over the Nova Scotian Shelf and in the Gulf of Maine. Mar Ecol Prog Ser 426:105–118. https://doi.org/10.3354/meps09002
- Speer JH (2010) Fundamentals of tree-ring research. University of Arizona Press, Tucson
- Stokes MA, Smiley TL (1996) An Introduction to tree-ring dating. University of Arizona Press, Tucson
- Strom A, Francis RC, Mantua N, Miles EL, Peterson DL (2004) North Pacific climate recorded in growth rings of geoduck clams: a new tool for paleoenvironmental reconstruction. Geophys Res Lett 31(L06206):1–4



Sutton RT, Hodson DL (2005) Atlantic Ocean forcing of North American and European summer climate. Science 309:115–118. https://doi.org/10.1126/science.1109496

- Thomas AC et al (2017) Seasonal trends and phenology shifts in sea surface temperature on the North American northeastern continental shelf. Elem Sci Anthropocene. https://doi.org/10.1525/journal.elementa.240
- Thomson DJ (1982) Spectrum estimation and harmonic analysis. Proc IEEE 70:1055–1095. https://doi.org/10.1109/PROC.1982.12433
- Torence C, Compo GP (1998) A practical guide to wavelet analysis. Bull Am Meterol Soc 79:61–78
- Townsend DW, Ellis WG (2010) Primary production and nutrient cycling on the Northwest Atlantic continental shelf. In: Liu K-K, Atkinson L, Quinones R, Talaue-McManus L (eds) Carbon and nutrient fluxes in continental margins: a global synthesis. IGBP book series. Springer, Berlin, pp 234–248
- Townsend DW, Thomas AC, Mayer LM, Thomas M, Quinlan J (2006) Oceanography of the Northwestern Atlantic Continental Shelf. In: Robin AR, Brink KH (eds) The sea. Harvard University Press, Cambridge, pp 119–168
- Townsend DW, Pettigrew NR, Thomas MA, Neary MG, McGillicuddy DJ Jr, O'Donnell J (2015) Water masses and nutrient sources to the Gulf of Maine. J Mar Res 73:93–122. https://doi.org/10.1357/002224015815848811
- Vautard R, Ghil M (1989) Singular-spectrum analysis: a toolkit for short, noisy chaotic signals. Phys D 35:395–424
- Wallace JM, Gutzler DS (1981). Teleconnections in the geopotential height field during the Northern Hemisphere winter. Mon Weather Rev 109:784–812. https://doi.org/10.1175/1520-0493(1981)109%3C0784:TITGHF%3E2.0.CO;2.
- Wanamaker AD et al (2008a) Coupled North Atlantic slope water forcing on Gulf of Maine temperatures over the past millennium. Clim Dyn 31:183–194. https://doi.org/10.1007/s00382-007-0344-8
- Wanamaker AD Jr, Heinemeier J, Scourse JD, Richardson CA, Butler PG, Eiriksson J, Knudsen KL (2008b) Very long-lived mollusks confirm 17th century AD tephra-based radiocarbon reservoir ages for North Icelandic shelf waters. Radiocarbon 50:399–412. https://doi.org/10.1017/S0033822200053510

- Wanamaker AD Jr, Butler PG, Scourse JD, Heinemeier J, Eiriksson J, Knudsen KL, Richardson CA (2012) Surface changes in the North Atlantic meridional overturning circulation during the last millennium. Nat Commun 3:899. https://doi.org/10.1038/ncomms1901
- Wanamaker AD Jr, Gillikin DP (2018) Strontium, magnesium, and barium incorporation in aragonitic shells of juvenile *Arctica islandica*: insights from temperature controlled experiments. Chem Geol. https://doi.org/10.1016/j.chemgeo.2018.02.012
- Wanamaker AD, Hetzinger S, Halfar J (2011a) Reconstructing mid- to high-latitude marine climate and ocean variability using bivalves, coralline algae, and marine sediment cores from the Northern Hemisphere. Palaeogeogr Palaeoclimatol Palaeoecol 302:1–9. https://doi.org/10.1016/j.palaeo.2010.12.024
- Wanamaker AD, Kreutz KJ, Schöne BR, Introne DS (2011b) Gulf of Maine shells reveal changes in seawater temperature seasonality during the Medieval Climate Anomaly and the Little Ice Age. Palaeogeogr Palaeoclimatol Palaeoecol 302:43–51. https://doi.org/10.1016/j.palaeo.2010.06.005
- Wigley TML, Briffa KR, Jones Pd (1984) On the average value of correlated time series, with application in dendroclimatology and hydrometeorology. J Appl Meteorol Climatol 23:201–213
- Witbaard R (1997) Tree of the sea. The use of internal growth lines in the shell of *Arctica islandica* (Bivalvia, Mollusca) for the retrospective assessment of marine environmental change. Ph.D., Rijksuniversiteit Groningen
- Witbaard R. Duineveld GCA, de Wilde PAWJ (1997) A long-term growth record derived from Arctica islandica (Mollusca, Bivalvia) from the Fladen Ground (northern North Sea). J Mar Biol Assoc UK 77:801–816. https://doi.org/10.1017/S002531540 0036201
- Wolter K, Timlin MA (1998) Measuring the strength of ENSO events—how does 1997/98 rank?. Weather 53:315–324
- Woollings T, Hannachi A, Hoskins B (2010) Variability of the North Atlantic eddy-driven jet stream. Q J R Meteorol Soc 136:856–868. https://doi.org/10.1002/qj.625
- Yamaguchi DK (1991) A simple method for cross-dating increment cores from living trees. Can J For Res 21(3):414–416

